university of groningen / faculty of science and engineering

Design of a Setup to Monitor an Ultra-High Dose Rate Proton Beam for Clinical Applications

Author:
Lucas KINGMA
(S5348277)

Supervisor:
prof. Alexander Gerbershagen
Second examiner :
prof. Peter Dendooven

Bachelor's Thesis
To fulfill the requirements for the degree of
Bachelor of Science in Applied Physics
at the University of Groningen

July 17, 2025

Contents

Abstract

A set-up is proposed for an optical system for Ultra-High Dose Rate (UHDR) dosimetry, where conventional diagnostic systems fail due to the high intensity proton beams. A scintillation method was used as a minimally invasive monitoring alternative. To maximize the light yield in the optimum wavelength range of the quantum efficiency of the camera and lens, low-pressure nitrogen gas was utilized. An electron-multiplying CCD camera was implemented for its sensitive nature allowing it to produce images with a low light yield. Lack of shielding and reflections in the set-up lowered the quality of the images, resulting in the production and testing of an improved design. Multiple parameters were varied to test if the set-up works for various conditions. For the first design, the exposure times were 1 and 10 s, the gains were 1 s and 50, the beam currents were 46 nA and 86 nA, the pressures were $5 \cdot 10^{-4}$ $mbar$ and $1.1 \cdot 10^{-1}$ $mbar$. The beam currents could not be increased further due to issues with the beam, resulting in larger than anticipated exposure times having to be used. The gain, a parameter that multiplies the received signal, shows great promise in improving the signal to noise ratio for light emission. And the pressure was kept low to keep scattering to a minimum. For the second experiment, the shielding had improved, resulting in less background radiation. Additionally, the set-up was tested with beam currents of 6 nA and 60 nA. The pressure and gain were increased to 110 $mbar$ and 100, respectively. As a consequence of imaging beams with a factor of 10 difference in the beam current, the exposure time was increased to 100 s for the beam of 6 nA. This confirmed the linear scaling of the beam current and the exposure time on the light yield. Further tests should be done to research the boundaries of the proportionality of all four parameters.

1 Introduction

In approximately half of the treatments for tumours, radiotherapy is used in one step of the process [1]. It is able to irradiate tumours at depths, or around organs, where surgery would struggle to reach. Consequently, it offers a valuable treatment possibility for patients with otherwise inoperable cancers with fewer side effects than chemotherapy.

Radiotherapy can be split into photon therapy and charged-particle therapy [2], where charged-particle therapy is ideal for an accurate treatment due to the differing dose distributions of the two techniques, as can be seen in Figure 1. The dose distribution of the photon beam is mainly focused on the region a short distance behind the skin, whereas the dose distribution of the proton beam is concentrated at the end of the beam in the Bragg peak. The Bragg peak, as seen in Figure 1, is a sharp rise and fall of the delivered dose at the end of the beams path. The Bragg peaks depth can be manipulated by changing the energy, where the higher the initial beam energy, the deeper the Bragg peak will deliver its dose. Due to the Bragg peak's characteristics, the dose is able to be better concentrated in the tumour with only a fraction of the distributed energy before the tumour and virtually zero radiation reaching deeper tissues. Resulting in a decrease in the probability of developing side effects due to a more accurate dose distribution. This is especially advantageous when the tumour is close to sensitive organs.

Charged-particle therapy consists of two main techniques: Passive Scattering Therapy (PST) and Pencil Beam Scanning (PBS). For PST, scattering material is placed in the path of the beam to spread the beam, thereupon collimators and compensators tailor the beam shape to the tumour. A set of range modulator wheels or ridge filters are used to spread out the Bragg peak [3]. Whilst PST irradiates the entire tumour all at once, PBS irradiates a narrow spot. For PBS, the beam is very thin and its transverse position is altered by scanning magnets. By varying the energy of the beam to alter the depth of the Bragg peak and sweeping the beam spot over the tumour at each depth, the whole tumour is irradiated. Due to improved selectivity of the dose distribution and the more recent feasibility of conformal dose distributions, PBS has started to replace PST in clinical use [4].

Ultra-high dose rate (UHDR) radiotherapy is radiotherapy technique that utilizes a dose rate of 30 Gy/s or higher, dwarfing normal dose rates of less than 0.3 Gy/s [5][6]. Considering that the full dose remains constant in all techniques, the irradiation times can decrease by three or more

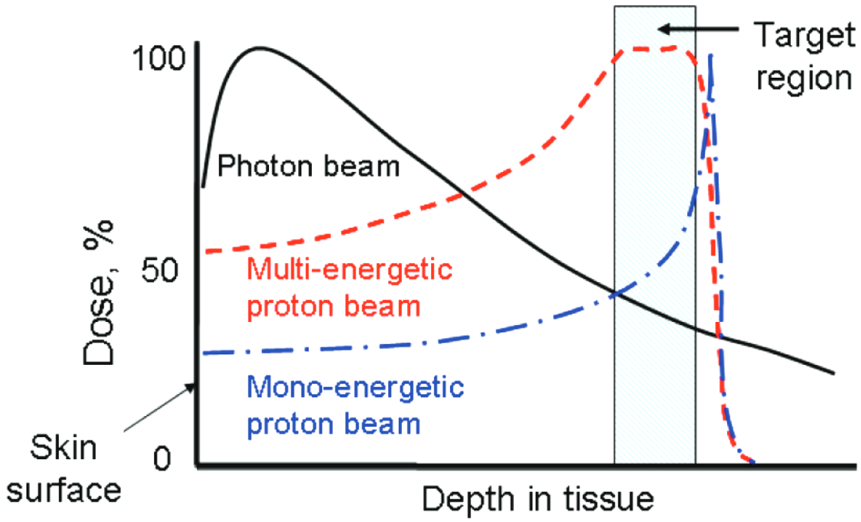

Figure 1: A comparison of dose-depth profiles for photon and proton therapies [2].

orders of magnitude, greatly diminishing the issue of a moving patient. In addition to the accelerated process, UHDR radiotherapies with a dose rate higher than 40 Gy/s have been found to generate the FLASH effect [5]. The FLASH effect (FE) was first discovered by Dewey and Boag (1959) [7], however it was not until Favaudon et al. (2014)[6] reported on their findings that FLASH-RT started to be investigated more actively. Favaudon reported on the reduction of early and late complications affecting healthy tissues after the elimination of a lung tumour compared to conventional radiotherapy, although the eradication of the tumour was just as efficient as with conventional irradiation. However, the workings of the FE are not yet fully understood, making it a hot topic in current research [5].

There is current research into the FE and thus methods are being developed towards enabling reliable UHDR irradiation at a clinical standard. In addition to the FE, there are benefits of using UHDR. Mainly, patient mobility is an issue during conventional radiation. Due to the decreased irradiation time, the treatments takes less than 100 ms. Consequently, younger patients, elderly or patients with a condition (i.e. Parkinson's disease) will be less prone to movement based errors. And perhaps more significant, the treatment is able to happen in between heart beats and breaths, drastically reducing motion uncertainties.

For UHDR to be implemented clinically, it is crucial to reliably and accurately monitor beam position and dosimetry. However, due to the high intensity of the beam, the usual ways of monitoring a beam, via ionisation chamber or wire chamber, will not work. Both techniques experience saturation caused by UHDR [8][9][10]. Therefore, large correction factors or computation should be adopted. These corrections bring errors with them and, most importantly, consume time. Ergo, this paper aims to design a set-up to image a UHDR proton with minimal disturbance to the beam, whilst not needing time-consuming computations. For this purpose, a low-pressure scintillation gas is adopted. As demonstrated by Forck et al. [11], the beam causes scintillation of gas molecules, which releases an photon that is monitored by a CCD camera. The usage of gas ensures minimal energy and flux loses to the beam.

In addition to the scintillation gas, care was given to the optical system attached to the camera. The degree to which light is detected depends on the material of the lens, the quantum efficiency of the CCD camera, and the type and pressure of the scintillation gas. Thus, this paper proposes a tested set-up design for imaging a high-intensity proton beam, with an extensive review of its optical system.

2 Background Literature

2.1 Scintillation

When an electron of a molecule gets excited, promptly de-excites, and releases a photon, it is called luminescence [12]. This luminescence is split up into multiple categories depending on what excites the initial electron. For instance, luminescence produced with an electron beam as the mode of excitation is called cathodoluminescence and if it originates from an electric field it is called electroluminescence. This paper will focus on radioluminescence, or scintillation, which originates from ionising radiation such as the proton beam used in this paper. Additionally, each molecule has an unique emission spectra, emitting differing wavelengths and relative intensities [11]. Thus, when imaging the emission, the scintillation gas used should be considered along with the quantum efficiency of the lens and the camera.

2.2 Optics

2.2.1 Field of View

The field of view can be described as either an angle or a length; for convenience, these will be called angle of view (AOV) and length field of view (LFOV), respectively.

AOV is the angle at which a camera is able to create an image. With a smaller angle, the image will become narrower and with a bigger angle, it becomes wider. Equation 1 gives the AOV given by an angle α. It can be seen that the AOV depends only on s_{sensor}, which is the size of the sensor horizontally, vertically, or diagonally, and the focal point, f. The chosen direction of s_{sensor} gives an AOV value in the same direction. Consequently, this is the AOV as can be imaged by the sensor, as opposed to the angle of coverage, which is the angle the lens is able to view.

$$\alpha = 2arctan(\frac{s_{sensor}}{2f}) \tag{1}$$

LFOV is the length of the object that is imaged by the camera, as shown in Figure 2. As can be expected, this depends on the AOV and the distance the camera is from the object. This dependence is shown in equation 2. Consequently, the LFOV can be changed as needed by moving the camera to

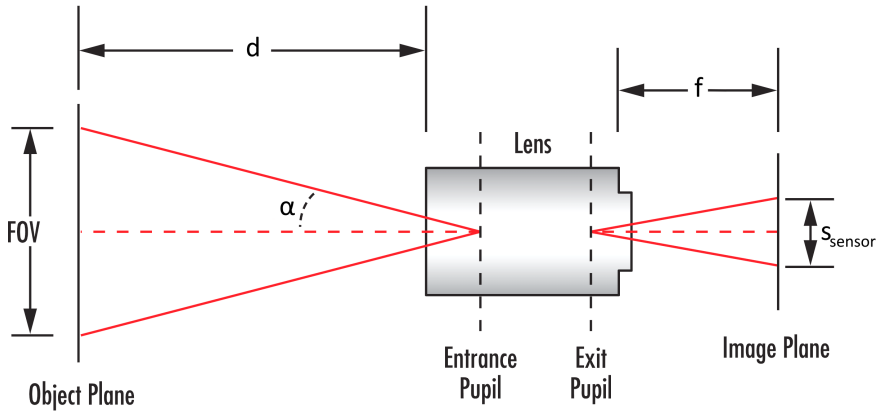

Figure 2: A schematic image that explains the field of view using the sensor size, s_{sensor}, the focal point, f, the focusing distance, d, and the angle, α.

or away from an object.

$$l = 2dtan(\frac{\alpha}{2}) \tag{2}$$

Here, l is the LFOV, d is the distance from the camera to the object, and α is the AOV.

2.2.2 Depth of Field

The depth of field is the range of distances around the focusing distance where the resolution of the image is considered sufficient and any objects imaged outside the depth of field will be considered blurry. With perfect lenses and infinitesimally sized pixels, only at the focusing distance will the image be perfectly sharp, with other distances resulting in an amount of blur depending on the distance from the focusing distance. This would result in a depth of field of 0 m, which results in only 2 dimensional objects being sharp in the image and having no margin of freedom when focusing. To get a depth of field larger than zero, the circle of confusion is of use. The circle of confusion, also called the blur spot, is the circle that is obtained by making a cross section of the cone of light at an arbitrary point after the lens, as can be seen in Figure 3. The chosen circle size is the amount of blur that is allowed in the image, and the depth of field is the entire range between the two circles of confusion, in front and behind the focusing distance. The circle of confusion can be taken as the size of a single camera pixel, so blurring between pixels does not occur. Mathematically, the depth of field can be described by formulae (3) and (4).

$$DoF_{farlimit} = \frac{H \cdot d}{H - (d - f)} \tag{3}$$

$$DoF_{nearlimit} = \frac{H \cdot d}{H + (d - f)} \tag{4}$$

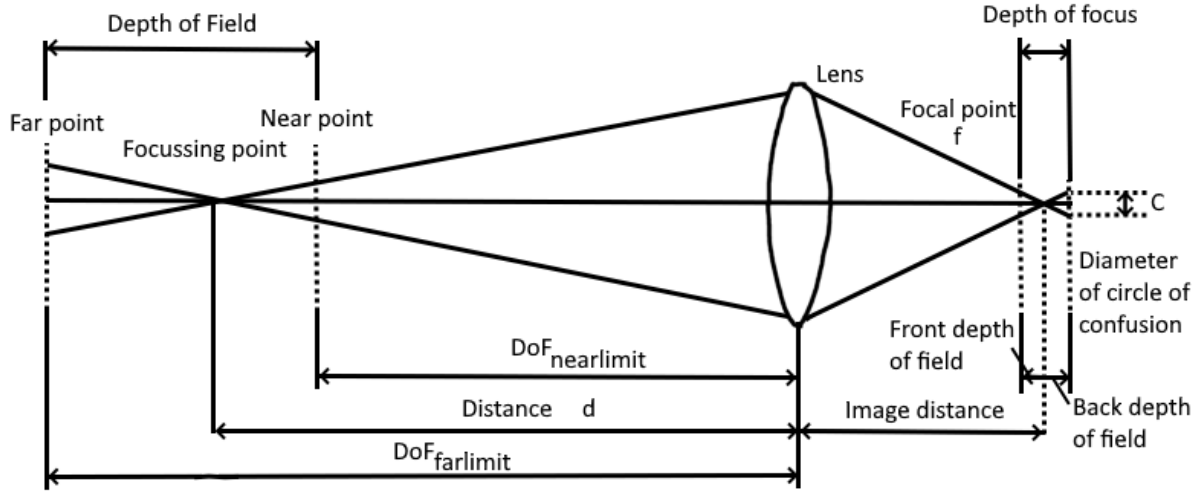

Figure 3: A visual representation of the circle of confusion and how the depth of field is dependent on it [13].

Here, d is the focusing distance, and H is the hyperfocal distance, which is the distance to a point of fixation at which the $DoF_{farlimit}$ goes to infinite[14]. The hyperfocal distance can be calculated with equation (5).

$$H = f + \frac{f^2}{N \cdot C} = f + \frac{f \cdot D}{C} \tag{5}$$

Where N is the f-number or the f-stop, C is the circle of confusion, and D is the diameter of the aperture.

2.3 Camera Settings

2.3.1 Exposure Time

The exposure time is the time the camera exposes the camera chip to light. During this time, the cumulative signal, received by the camera chip, makes up the image. This results in the exposure time being proportional with the signal, i.e. an image with an exposure time of 1 second receives double the light compared to an image with an exposure time of half a second.

2.3.2 Gain

When the camera chip detects a photon, a photoelectron is released [15]. These photoelectrons are stored during the time the image is taken and after the amount is measured and turned into a digital signal. This process is called the 'gray level' or analog-to-digital unit. The gray level contains the values read out by the computer and shows up as the pixels' intensity. The gray level goes up to $2^n - 1$, where n is the number of bits. Therefore, a 16-bit camera will have a maximum gray level of $2^{16} - 1 = 65535$. Each gray level does not necessarily correspond to one photoelectron; instead, the amount of photoelectrons that correspond to one gray level is decided by the gain. Assuming the gain is linear, if a camera has a gain of 10 $e^-/gray$, it will read out 1 gray level per 10 stored photoelectrons.

Electron-multiplying camera's, like the camera used in this paper, are able to multiply photoelectron with the 'multiplier gain'. This multiplication divides the gain value, so electron-multiplying cameras can even have a gain of 0.03 $e^-/gray$ [15]. In the future, when talking about a gain of x, the multiplier gain is meant.

3 Experimental Set-up

The setup, found in Figure 4, consisted of a pressure-controlled gas block, a meter-long tube, a zoom lens, and a EMCCD camera. The gas block was filled with a low-pressure nitrogen gas, and it had an airtight foil at both ends to allow the beam to pass through. In the middle of the block, there was a hole at a 90 degree angle of the beam aimed at the camera, which was blocked by a window so the light can go through but the gas stayed inside. Inside of the gas block was a cylinder that was darkened with a black foil, so light from outside the block or from the other half of the block could not enter. The gas block Between the gas block and the camera was a tube that shielded the camera from other sources of light. The distance between the camera and the gas block was a measure against beam-induced background radiation utilizing the inverse-square law. The camera was an electron-multiplying CCD camera, which means that it is extremely sensitive to light, as discussed in Chapter 2.3.2. It needed to be sensitive to light, because not a lot of light was expected. The camera was controlled with μmanager, an open source software. The software adopts PIcam to control the camera, the driver made by the manufacturers of the used camera. In μmanager, the exposure time and gain were changed. Nitrogen was used during the experiment since it emits wavelengths that correspond to an acceptable quantum efficiency of the camera. However, the main wavelength emitted by nitrogen has a poor transmittance percentage when using this specific lens.

3.1 Tools and Technologies

As mentioned in Chapter 3, a zoom lens, a camera, and μmanager were used to image the beam. The focal point of the lens could be changed from 12.5 *mm* to 75 *mm*, depending on the required

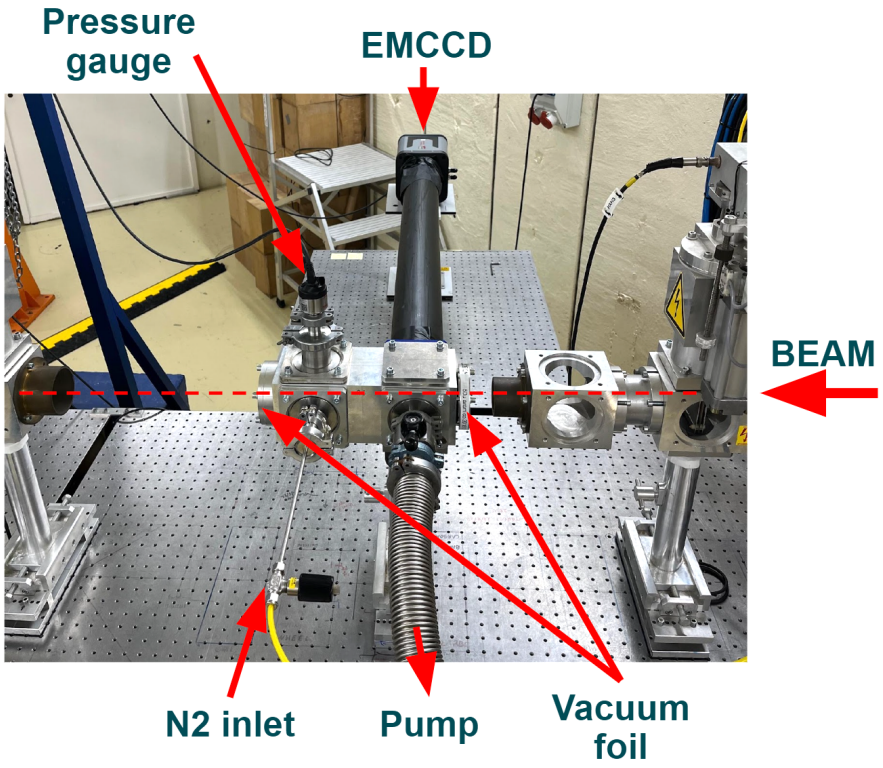

Figure 4: An image of the set-up; it shows the pressure gauge, the EMCCD camera, the N_2 inlet, where the pump is attached; the beam runs horizontal through the middle of the image.

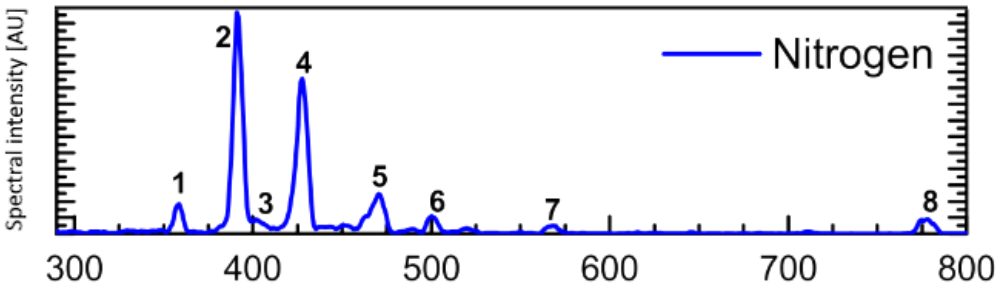

Figure 5: The emission spectrum for nitrogen; It displays the spectral intensity versus the wavelength of the emitted photon.

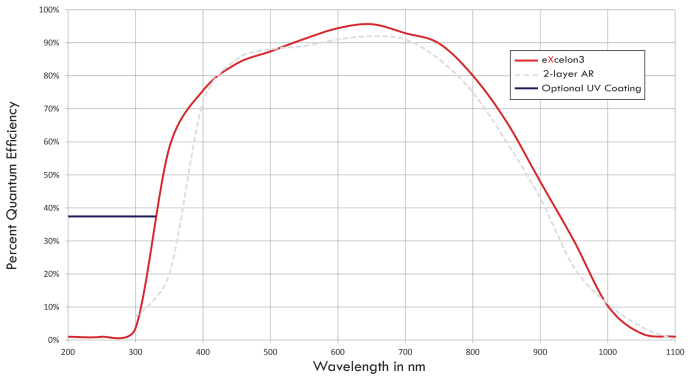

(a) The quantum efficiency curve of the eXcelon3 camera used in the experiment

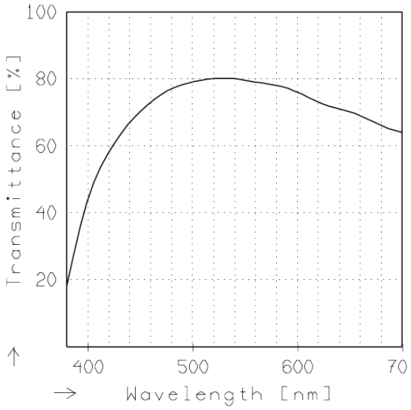

(b) The spectral transmittance of the lens used in the experiment

Figure 6: Image 6a shows the quantum efficiency of the ProEM®-HS:512BX3 camera used in the experiment. Image 6b shows the transmittance of the Schneider Optics Variogon 1.8/12.5-75mm lens used in the experiment

magnification. A focal point of 75 *mm* was used to make the beam as large as possible in the image. The focal point, together with the f-number, are values that change the size of the depth of field. To obtain the desired depth of field, the f-number could also be changed. Its values range from 1.8 to 16. However, due to expecting a small amount of light, the aperture was desired to be large for a better light yield. Consequently, a f-number of 1.8 was chosen, despite resulting in a smaller depth of field as it was decided the strength of the signal was more important than some depth defocusing of the produced light.

The camera used was the ProEM-HS 512 eXcelon3, which has a sensor of 512X512 square pixels with a width of 16 μm. It is able to apply a gain of up to 1000 when imaging. However, a gain of 50 was the highest gain used during the first experiment, in order not to accumulate dead pixels.

3.2 Image Processing

3.2.1 Median Filter

Since the camera is quite sensitive, there will be noise in the background. And as a consequence of the beam, neutrons can appear which will go through the camera casing and hit the chip; in images

these will appear at random places as high-intensity pixels. To denoise and remove the high-intensity pixels, a mean filter or a median filter can be used. Both filters examine a n by n grid around every pixel (e.g. 3x3, 5x5, etc.) and replace the value with the mean or median intensity of all surrounding pixels in the grid, respectively. A nine by nine grid is chosen, and not a bigger grid, as the bigger the grid is, the more resolution is lost. The mean filter has the issue of being very sensitive to overshoots. As it is a 16-bit system, the values can range from 0 to $65,535$. The background radiation causes unfavourable overshoots, especially for mean filters, however dead pixels can appear conjointly with them. These dead pixels are pixels in the camera chip that have seized working. If there is a dead pixel, which is shown as the maximum value, all pixels around it will get a greatly exaggerated value above what it is. This exaggeration will not happen with a median filter, unless multiple high-intensity pixels neighbour each other. Consequently, a median filter will be used for image processing.

3.2.2 Clipping

If neutrons or gamma rays hit the camera, the hit pixels will receive a lot of signal at once. In addition, this background radiation will not necessarily be fully absorbed by the camera, meaning that one neutron is able to hit more than a singular pixel. Consequently, a single neutron hitting the camera chip raises the maximum intensity of the image to values significantly higher than the values of the pixels that are desired to be observed. This might result in images in which only the pixel hit by background radiation is distinguishable from the read noise of the camera. To correct for the background radiation, the image can be clipped. Clipping changes what range of intensity values are assigned to the colour palette of the displayed image. Consequently, All pixels with values outside of this range are set to the value of its nearest extreme. Thus, all values with originally larger, or lower, pixel intensities will be the same shade as the nearest extreme. For the first experiment, all images will be clipped between 600 *AU* and 750 *AU*.

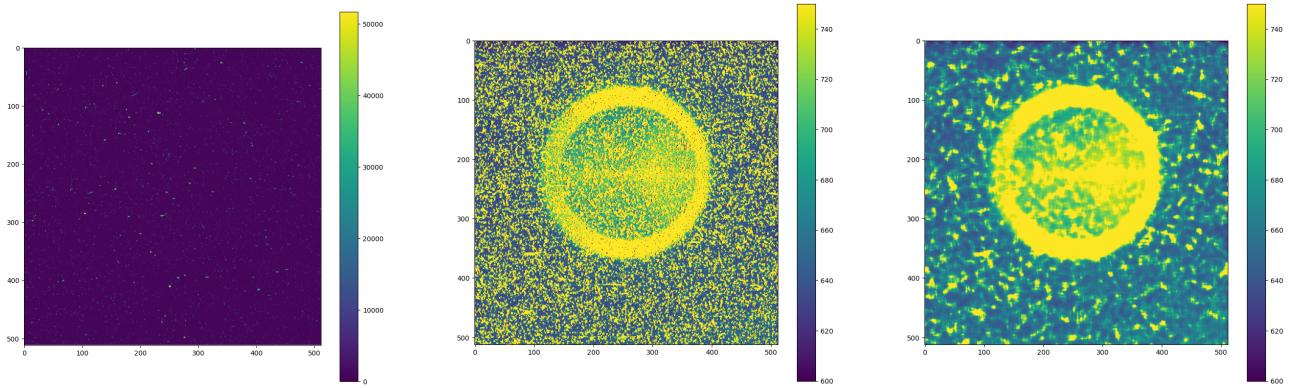

(a) Unclipped image without a median filter

(b) Clipped image without a median filter

(c) Clipped image with a 9 by 9 median filter applied

Figure 7: All three images show the same image; Figure 7a shows the image unclipped and without having a median filter applied to it, Figure 7b shows the image being clipped between the values 600 *AU* and 750 *AU* with out a median filter being applied, and Figure 7c shows the image being clipped between the values 600 *AU* and 750 *AU* with a nine by nine median filter applied to it.

3.3 Improved Design

After the first experiment, several shortcomings were found with the earlier described set-up. The shortcomings, as can be seen in Chapter 4, are mainly the result of a lack of shielding and the aforementioned cylinder. Consequently, shielding was placed around the camera and the cylinder was swapped out with a new design that, instead of being perpendicular, was parallel to the tube. Due to having better shielding, the gain was increased to a maximum of 100, as there was less background radiation to cause dead pixels. Consequently, the maximum clipped value had to be increased to 3000 AU, otherwise the image would show no distinction of pixel intensities in the beamline. In Chapter 5, the reasoning behind the change of the cylinder will be discussed. The altered design can be seen in Figure 8.

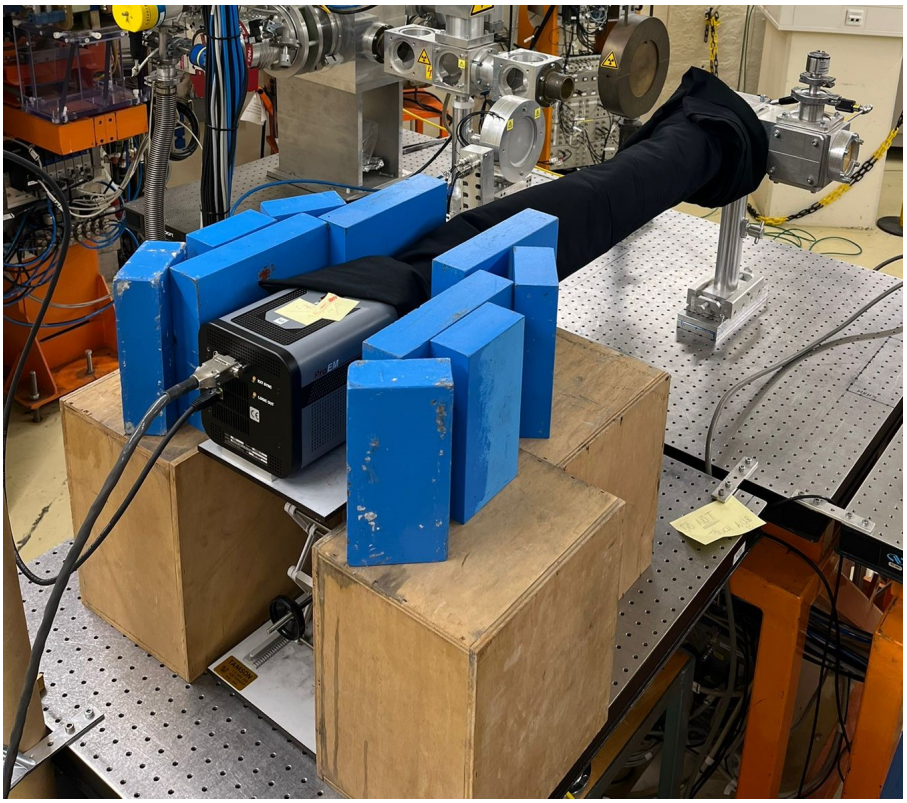

Figure 8: An image of the improved set-up design; compared to the old set-up, the improved design contains shielding in the form of lead blocks and as an extra measure a blackening cloth was put around the tube.

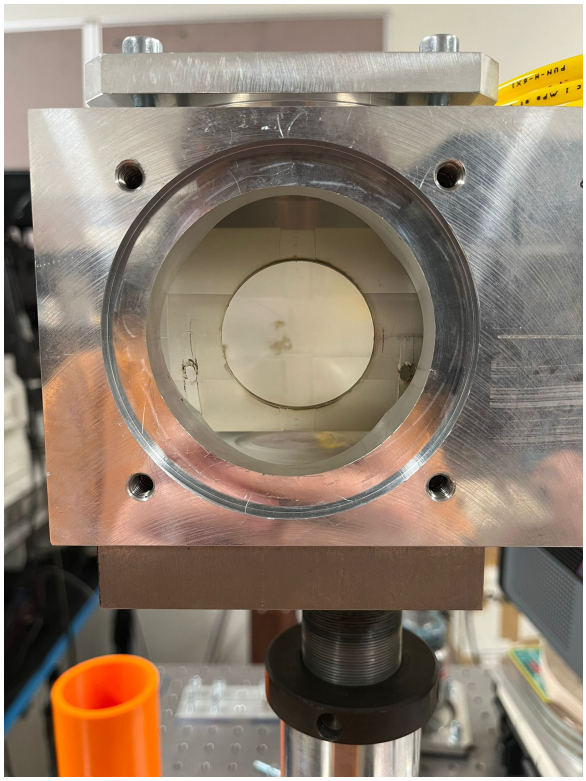

(a) The cylinder of the old set-up that is parallel with the beam

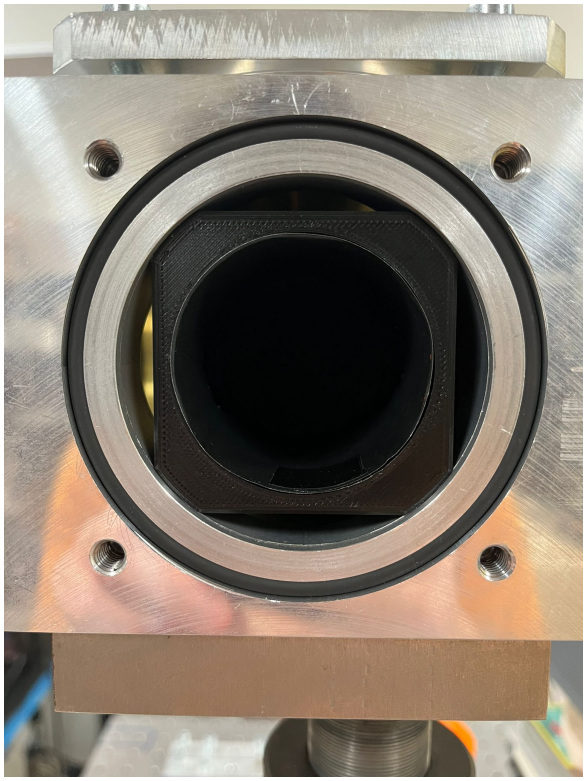

(b) The cylinder of the improved set-up that is perpendicular to the beam

Figure 9: Comparison between the two cylinders; Figure 9a shows the old cylinder that is parallel with the beam, as a result there is distance between the cylinder and glass that was placed in the exit of the gas block, note that during the experiment the inside of the cylinder was darkened. Figure 9b shows the new cylinder that is perpendicular to the beam, resulting in less space between the glass and less reflecting light.

4 Results

4.1 Exposure Time

Figures 10a and 10b show the effect of the exposure time; An exposure time of ten seconds should roughly give ten times more signal than an exposure time of one second, which is difficult to recognize due to the read noise and the image being clipped. The greatest increase can be seen in the back ground radiation; however, the torus becomes clearer with an increased exposure time. The 2D bright torus is visible as a result of light reflection within the pressurized block. The image taken with one second of exposure time shows only noise and a faint outline of a torus and the image with ten seconds of exposure time shows a clear torus in the middle along with a horizontal line at the height of the beam. Due to the better appearance of the beam, ten seconds was regarded as the more suitable exposure time to obtain observable data, in spite of the increased background noise. Thus, all remaining images were taken with an exposure time of ten seconds.

4.2 Gain Multiplier

For comparison, images were produced with gains of one and 50, an exposure time of 10 s, an beam current of 86 nA, and for a pressure of $5 \cdot 10^{-4}$ $mbar$. Figures 11a and 11b show the increase in signal, both intended signals and noise, as the gain increases. The image with a gain of one presents little of both the beam and the background radiation but does show the torus, albeit of low intensity. The image made with a gain of 50 shows increased intensity. It shows a horizontal line at the location of the beam running through the middle of the torus. Additionally, it contains a cluster of high intensity pixels on the right side in the torus.

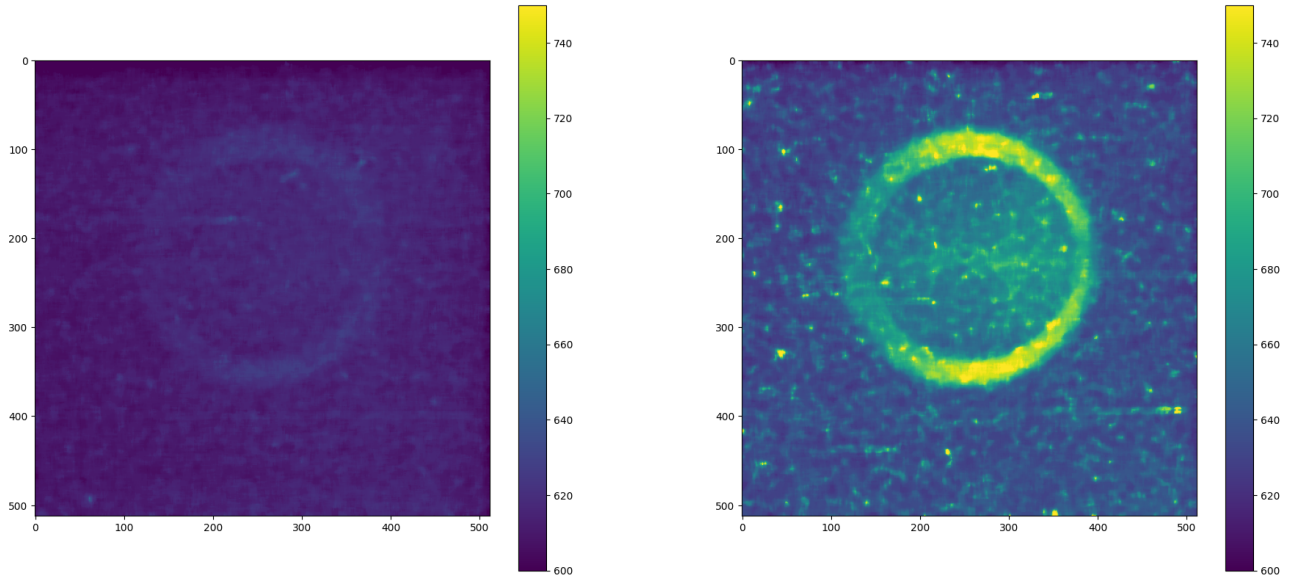

(a) Image taken with an exposure time of 1 s

(b) Image taken with an exposure time of 10 s

Figure 10: Images taken of the beam with a beam current of 46 nA, with a pressure of $1.1 \cdot 10^{-1}$ $mbar$, and with a multiplier gain of 50. Both images are clipped between the values 600 AU and 750 AU. The left image, (a), was taken with an exposure time of 1 s compared to the image on the right, (b), taken with an exposure time of 10 s.

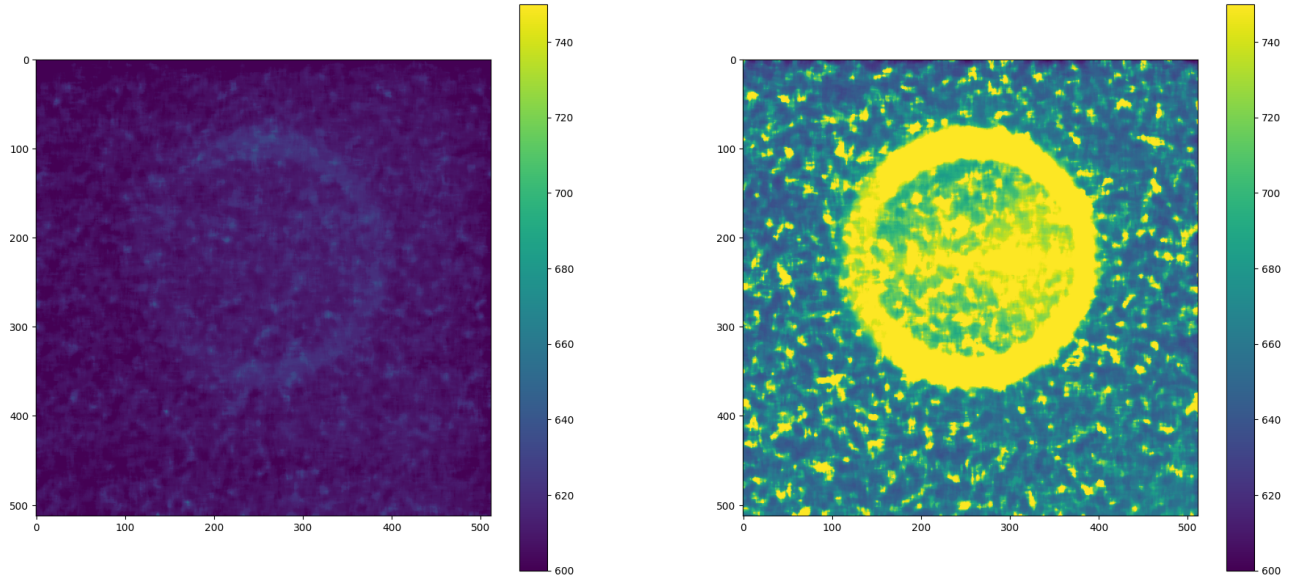

(a) Image taken with a gain of 1

(b) Image taken with a gain of 50

Figure 11: Images taken of the beam with a beam current of 46 nA, with a pressure of $1.1 \cdot 10^{-1}$ $mbar$, and with an exposure time of 10 s. Both images are clipped between the values 600 AU and 750 AU. The left image, (a), was taken with a gain of 1 compared to the image on the right, (b), taken with a gain of 50.

4.3 Beam Current

The two beam currents used were 46 nA and 86 nA. The images taken with 46 nA contain fewer high-intensity pixels than when taken with a 86 nA beam current, as can be seen in Figures 12a and

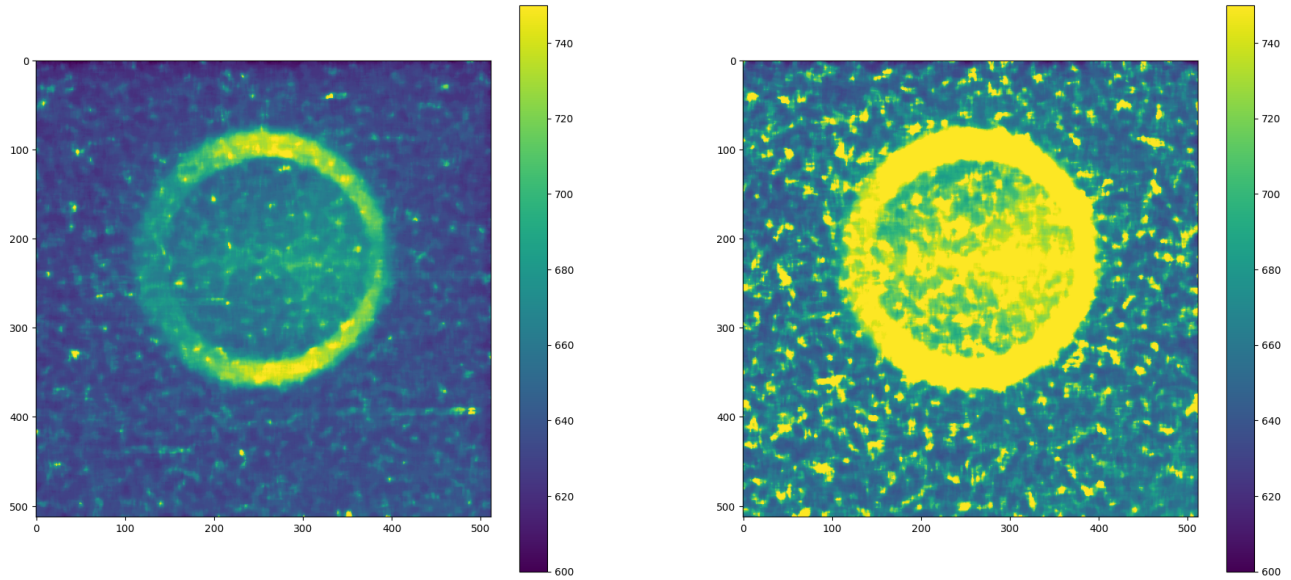

(a) Image taken with a beam current of 46 nA

(b) Image taken with a beam current of 86 nA

Figure 12: Images taken of the beam with a with a pressure of $1.1 \cdot 10^{-1}$ $mbar$, a gain of 50, and with an exposure time of 10 s. Both images are clipped between the values 600 AU and 750 AU. The left image, (a), was taken with a beam current of 46 nA and the image on the right, (b), was taken with a beam current of 86 nA.

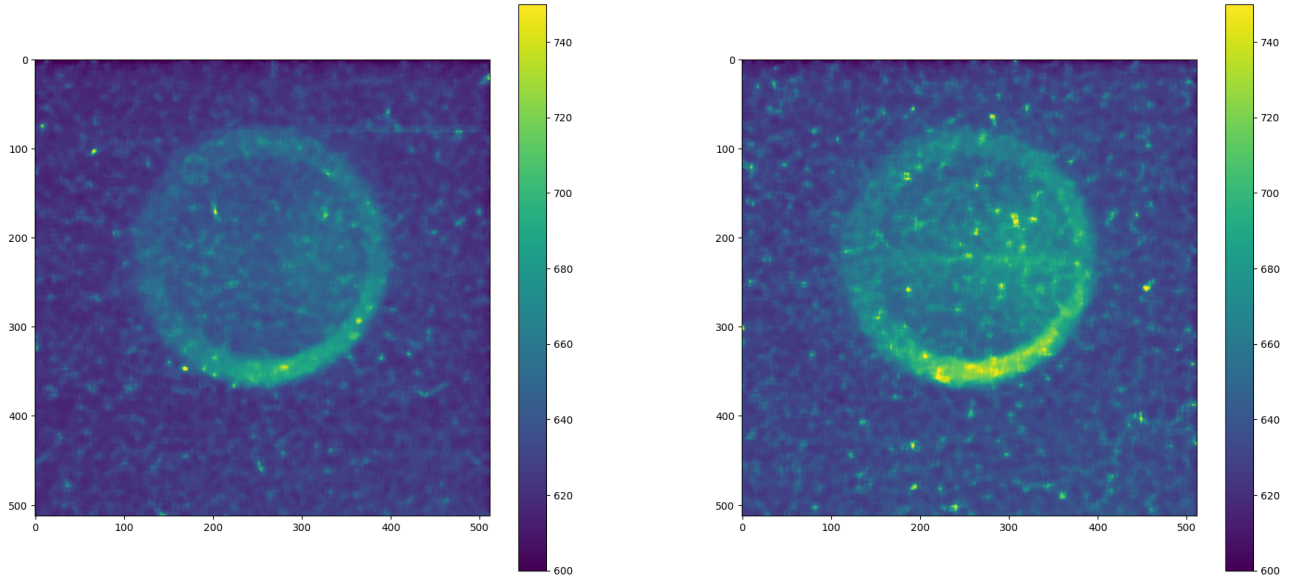

(a) Image taken with a pressure of $5 \cdot 10^{-4}$ *mbar*

(b) Image taken with a pressure of $1.1 \cdot 10^{-1}$ *mbar*

Figure 13: Images taken of the beam with a beam current of 46 *nA*, a gain of 50, and with an exposure time of 10 *s*. Both images are clipped between the values 600 *AU* and 750 *AU*. The left image, (a), was taken with a pressure of $5 \cdot 10^{-4}$ and the image on the right, (b), was taken with a pressure of $1.1 \cdot 10^{-1}$ *mbar*.

12b. In both images, the beam shows up, although with high intensity in Figure 12b. Additionally, in both images the right side in the torus is more signal than on the left side.

4.4 Pressure

The difference in pressure between Figure 13a is more than 500 times less than 13b. However, there is a smaller difference in the amount of signal received by the camera in both images. The torus is clearly visible in both images, although it is less visible in Figure 13a. Despite the small difference between the two images, only Figure 13b shows a brighter line in the middle of the torus where the beam is.

4.5 Improved Set-up

The two improvements made to the set-up were: more shielding around the camera and the alternative cylinder in the gas block, as can be seen in Figures 8 and 9b. This Resulted in less background noise and a missing torus, as seen in Figures 14a and 14b. The images were made with a higher gain and pressure compared to the images made with the older set-up. Consequently, the images have received more signal and had to be clipped with a higher maximum value of 3000. The images were both made with a gain of 100 and a pressure of 100 *mbar* and differed in both the exposure time and beam current. Figure 14a was taken with an exposure time of 100 *s* and a beam current of 6 *nA* and Figure 14b was taken with an exposure time of 10 *s* and a beam current of 60 *nA*. As mentioned in Chapter 4.1, an exposure time of 10 *s* was the standard during the experiments. However, to confirm the expectations about the dependence of the light yield on the beam current and exposure time, the parameters of Figure 14a were decided upon. Comparing Figures 14a and 14b, little difference can

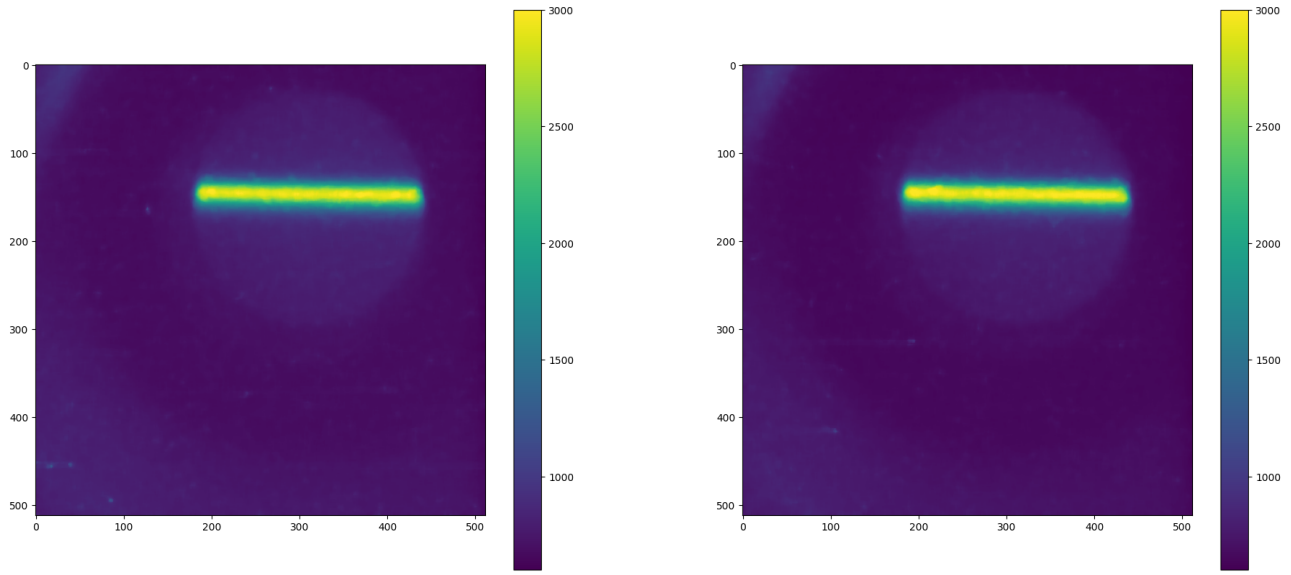

(a) Image taken with a beam current of 6 *nA* and an exposure time of 100 *s*

(b) Image taken with a beam current of 60 *nA* and an exposure time of 10 *s*

Figure 14: Images taken of the beam with a gain of 100 and with a pressure of 110 *mbar*. Both images are clipped between the values 600 *AU* and 3000 *AU*. The left image, (a), was taken with a beam current of 6 *nA* and an exposure time of 100 *s* and the image on the right, (b), was taken with a beam current of 60 *nA* and an exposure time of 10 *s*.

be observed between the two, as will be discussed in Chapter 5.6.

5 Discussion

5.1 Exposure Time

The images were taken with an exposure time of one second or ten seconds, with more useful data resulting from the latter. This is currently in direct opposition to the purpose of the set-up: Imaging a UHDR beam with parameters where the FLASH effect is able to occur, meaning the irradiation time transpires in less than 100 ms. To optimise the desired exposure time, factors such as gain, beam current, and pressure should be increased. However, an increase in gain and pressure past the values used in this experiment might not be ideal. As the gain increases, so does the intensity of the neutrons and gamma rays. Further tests should be performed to test the limit of the gain until the image quality drops too far. Increasing the pressure too much would alter the beam by scattering it, conflicting with the desire to produce a minimally invasive set-up.

5.2 Gain

Comparisons of gains of 1 and 50 show an increase in intensity of every pixel, except for the readout noise. The images with an increased gain display a greater ability to observe the beam, but also the background radiation. This displays the demand for more shielding that was implemented in the improved design. Figure 11a featured a cluster of light on the right side in the torus. This is expected to be light that backscattered from the foil at the end of the cylinder.

5.3 Beam Current

Figures 12a and 12b show an increase of roughly a factor of 2 when the beam current increased the same amount, suggesting a linearity between the beam current and the light emittance. Therefore, increasing the beam current would be an ideal approach to increase the amount of light emitted. The cyclotron used for this experiment is capable of delivering a beam current higher than 1000 nA, which did not occur due to restrictions with the beam. If the beam current and light yield remain linear, even at higher currents, this could allow for a shorter exposure time to be used. For example, with the improved set-up, an exposure time of 10 s and a beam current of 60 nA were utilized. If the current would increase to a FLASH intensity of around 1500 nA, then the exposure time could decrease to $10 \cdot \frac{60}{1500} = 0.4\ s$. With an increase of gain, it could be decreased even further, resulting in the desired exposure time for FLASH-RT.

5.4 Pressure

As mentioned in Chapter 4.4, the pressure utilized in Figure 13a is more than 500 times lower than the pressure used in 13b. However, this did not decrease the signal nearly as much as 500 times. This suggests that the proportionality of the pressure breaks down at higher pressures. However, more data are required to confirm the boundaries of its proportionality. More measurements with different intermediate pressures and different beam currents and beam energies should be examined.

5.5 Background Radiation and Noise

Due to the beam, a large amount of background radiation is released and hits the camera chip. This becomes more noticeable with increasing exposure time, gain, and beam current, as seen in Figures

10-12. Figures 10b and 12a show that some of the background radiation hits the beam at large angles, resulting in streaks of high-intensity pixels. The background radiation problem has partially been resolved using the improved set-up, which will be discussed in Chapter 5.6.

5.6 Improved Set-up

The images taken with the old set-up had two main issues: a lot of background noise and an undesired torus shape appearing form light reflections inside the gas block. The former was mitigated with lead shielding placed around the camera, as seen in Figure 8. A substantial part of the background radiation was stopped, as seen in Figure 14. The latter was fixed by swapping out the cylinder. The original cylinder had a few centimetres between it and the glass between the block and the camera. The light was most likely able to reflect from the glass back to the cylinder, resulting in a bright torus shape in the image as the outside of the cylinder was not darkened. A new cylinder was substituted for the old one, where the new design was perpendicular to the beam and touching the glass. Consequently, the torus has ceased appearing in the picture. Interesting to note, there are three places of different pixel intensity below 1500. An inner circle shows around the beam, which is the back side of the improved cylinder. The darker torus around the circle is most likely due to the blackened attachment that attaches the tube to the block, shown in Figure 9. And finally, the lighter blue part, seen in the bottom and top left corners, is expected to be the black tube between the block and the camera.

Both Figures 14a and 14b look nearly identical, which shows the proportionality of the beam current and the exposure time. Since Figure 14a was taken with a tenth of the beam current and was taken with an exposure time that is ten times greater compared to Figure 14b. This confirms beam current and exposure scale linearly at these values. To examine the proportionality of the gain or the pressure, more data is required.

5.7 Further Research Possibilities

To begin with, the proportionality of the pressure, the beam current, and the gain should be researched, to see if there is a lower and upper limit where it remains proportional. With the information, the upper limits should be used to produce an image with an exposure time less than 100 *ms*, since long exposure times are not as useful for UHDR radiotherapy where the FLASH effect is desired. Due to time and beam restrictions, these could not be done. Additionally, another lens with a higher focal point should be used to get a larger zoom. This would result in a larger image of the beam, which would make the relative size of the noise smaller, meaning smaller filters could be used. Furthermore, it would mean that the camera can be put further back from the beamline as an additional measure against background radiation.

6 Conclusion

6.1 Summary of Main Contributions

Although the images received with the first set-up have a lower quality compared to the images produced with the improved set-up, it showed that the set-up works, shows promise, and it does show the dependencies of the signal on exposure time, gain, beam current, and air pressure. The main faults were reduced with an improved set-up. Consequently, the quality of the images improved greatly. These images show the proportionality of the beam current and the exposure time. The proportionality of gain and pressure should be researched in the future, as should the limits of the proportionality of the beam current. Future improvements in the set-up include a lens with a higher focal point and a longer tube if needed.

6.2 Future Work

This work was a summary of the aid that I provided to my daily supervisor Thomas Fogg and he will continue the research as part of his PhD. He will continue to gather data to test the boundaries of the proportionality. He aims to use the light output as a diagnostic tool for UHDR radiotherapy.

Bibliography

[1] R. Baskar, K. A. Lee, R. Yeo, and K.-W. Yeoh, "Cancer and radiation therapy: Current advances and future directions," *International Journal of Medical Sciences*, vol. 9, p. 193–199, Feb 2012.

[2] P. Azimi and A. Movafeghi, "Proton therapy in neurosurgery: A historical review and future perspective based on currently available new generation systems," *International Clinical Neuroscience Journal*, vol. 3, p. 59–80, Sep. 2016.

[3] F. Bourhaleb, A. Attili, and G. Russo, "Monte carlo simulations for beam delivery line design in radiation therapy with heavy ion beams," in *Applications of Monte Carlo Methods in Biology, Medicine and Other Fields of Science* (C. J. Mode, ed.), ch. 7, Rijeka: IntechOpen, 2011.

[4] A. Michaelidesová, J. Vachelová, J. Klementová, T. Urban, K. Pachnerová Brabcová, S. Kaczor, M. Falk, I. Falková, D. Depeš, V. Vondráček, and M. Davídková, "In vitro comparison of passive and active clinical proton beams," *International Journal of Molecular Sciences*, vol. 21, no. 16, 2020.

[5] J. Farr, V. Grilj, V. Malka, S. Sudharsan, and M. Schippers, "Ultra-high dose rate radiation production and delivery systems intended for flash," *Medical Physics*, vol. 49, no. 7, pp. 4875–4911, 2022.

[6] V. Favaudon, L. Caplier, V. Monceau, F. Pouzoulet, M. Sayarath, C. Fouillade, M.-F. Poupon, I. Brito, P. Hupé, J. Bourhis, J. Hall, J.-J. Fontaine, and M.-C. Vozenin, "Ultrahigh dose-rate flash irradiation increases the differential response between normal and tumor tissue in mice," *Science Translational Medicine*, vol. 6, no. 245, pp. 245ra93–245ra93, 2014.

[7] D. L. Dewey and J. W. Boag, "Modification of the oxygen effect when bacteria are given large pulses of radiation," *Nature*, vol. 183, p. 1450–1451, 1959.

[8] F. Romano, C. Bailat, P. G. Jorge, M. L. F. Lerch, and A. Darafsheh, "Ultra-high dose rate dosimetry: Challenges and opportunities for flash radiation therapy," *Medical Physics*, vol. 49, no. 7, pp. 4912–4932, 2022.

[9] Y. Arimoto, N. Higashi, Y. Igarashi, Y. Iwashita, T. Ino, R. Katayama, M. Kitaguchi, R. Kitahara, H. Matsumura, K. Mishima, N. Nagakura, H. Oide, H. Otono, R. Sakakibara, T. Shima, H. Shimizu, T. Sugino, N. Sumi, H. Sumino, K. Taketani, G. Tanaka, M. Tanaka, K. Tauchi, A. Toyoda, T. Tomita, T. Yamada, S. Yamashita, H. Yokoyama, and T. Yoshioka, "Development of time projection chamber for precise neutron lifetime measurement using pulsed cold neutron beams," *Nuclear Instruments and Methods in Physics Research Section A: Accelerators, Spectrometers, Detectors and Associated Equipment*, vol. 799, pp. 187–196, 2015.

[10] N. Nagakura, K. Fujii, I. Harayama, Y. Kato, D. Sekiba, Y. Watahiki, and S. Yamashita, "Experimental verification of a gain reduction model for the space charge effect in a wire chamber," *Progress of Theoretical and Experimental Physics*, vol. 2018, p. 013C01, 01 2018.

[11] P. Forck, C. Andre, F. Becker, R. Haseitl, and B. Walasek-Höhne, "Beam induced fluorescence profile monitor developments," *HB 2010 - 46th ICFA Advanced Beam Dynamics Workshop on High-Intensity and High-Brightness Hadron Beams*, 01 2010.

[12] S. Beddar and L. Beaulieu, "Scintillation dosimetry," 2016.

[13] Z. Songnian, Z. Qi, L. Chang, L. Xuemin, S. Shousi, and Q. Jun, "The representation of visual depth perception based on the plenoptic function in the retina and its neural computation in visual cortex v1," *BMC neuroscience*, vol. 15, p. 50, 04 2014.

[14] K. N. Ogle and J. T. Schwartz, "Depth of focus of the human eye∗," *J. Opt. Soc. Am.*, vol. 49, pp. 273–280, Mar 1959.

[15] "Camera Gain — teledynevisionsolutions.com." https://www.teledynevisionsolutions.com/learn/learning-center/imaging-fundamentals/camera-gain/. [Accessed 10-07-2025].